Journal of Earth Science, *Vol. 30*, *No. 4*, *p. 809–822*, *August 2019* *ISSN 1674-487X*
Printed in China
https://doi.org/10.1007/s12583-017-0946-y

Differentiation of Continental Subduction Mode: Numerical Modeling

Tuoxin Yang[1], **Pengpeng Huangfu**[2], **Yan Zhang***[1]

1. *Guangdong Provincial Key Lab of Geodynamics and Geohazards*, *School of Earth Sciences and Engineering*, *Sun Yat-Sen University*, *Guangzhou* 510275, *China*; *Southern Laboratory of Ocean Science and Engineering*, *Zhuhai* 519082, *China*
2. *Key Laboratory of Computational Geodynamics*, *College of Earth Sciences*, *University of Chinese Academy of Sciences*, *Beijing* 100049, *China*

ABSTRACT: The convergence of the multi-layered continental lithospheres with variable and complex thermal and rheological properties results in various modes of continental collision with distinct deformation behavior of the lithospheric mantle. Using high-resolution thermo-mechanical numerical models, we systematically investigated the effects of crustal rheological strength and the convergence rate on the continental subduction mode. The model results reveal three basic modes of continental subduction, including slab break-off, steep subduction and continental flat-slab subduction. Whether lithospheric mantle of the overriding plate retreats or not during convergence enables the division of the first two modes into two sub-types, which are dominated by the crustal rheological strength. The mode of slab break-off develops under the conditions of low/moderate rheological strength of the continental crust and low convergence rate. In contrast, continental flat-slab subduction favors the strong crust and the high convergence rate. Otherwise, continental steep subduction occurs. The numerical results provide further implications for Geodynamics conditions and physical processes of different modes of continental collision that occur in nature.

KEY WORDS: continental subduction, slab break-off, steep subduction, continental flat-slab subduction, numerical modeling.

0 INTRODUCTION

Continental subduction/collision and mountain building generally occurs under the convergent forces of lateral ridge push and/or subducted slab pull (Turcotte and Schubert, 2002). At the beginning of continental collision, the continental crust may simply subduct together with the lithospheric mantle into the subduction channel, resulting in positive buoyancy against the downward drag. Consequently, the continental crust, especially the upper/middle crust, may be decoupled from the mantle lithosphere and finally exhume upward (Li F C et al., 2018; Burov et al., 2014a; Li, 2014; Warren, 2013; and references therein). Five possible continental collision scenarios have been proposed in the regimes with different kinematic and dynamic conditions: (1) simple shear in stable subduction (Li et al., 2010; Faccenda et al., 2008); (2) pure shear thickening (Burov et al., 2014b); (3) thickening and dripping into the deeper mantle due to Raleigh-Taylor instability (Conrad and Molnar, 1997; Houseman and Molnar, 1997); (4) folding model (Burg and Podladchikov, 2000; Cloetingh et al., 1999; Burov and Molnar, 1998); and (5) retreat of the downgoing plate (Gray and Pysklywec, 2012). Among these variable collisional modes, simple shear continental subduction may dominate at least at the beginning of continental collision, which can be further divided into two styles (Li et al., 2011): steep subduction versus flat subduction. The previous studies, especially dynamic modeling, mostly focus on the steep continental subduction channel (Burov et al., 2014a; Li, 2014; Warren, 2013; and references therein); however, the development and differentiation of continental subduction still remains enigmatic.

In this study, numerical models with variable crustal rheological strength and convergence rate are systematically constructed, aiming to explore the development and differentiation of continental subduction during convergence between two colliding continents. The numerical results reveal three basic modes of continental subduction as well as the corresponding geodynamic conditions and physical processes.

1 MODEL SETUP

Aiming to study the dynamics of continental subduction, we constructed large-scale numerical models (4 000 km×670 km, Fig. 1a) using the thermo-mechanical code "I2VIS" (Gerya and Yuen, 2003a), which is a combination of the finite difference method with marker-in-cell techniques. The details of the numerical methodology can be found in Huangfu et al. (2017). The models consist of a non-uniform 699×134 rectangular grid with a resolution varying from 2×2 km in the vicinity of the collision zone to 30×30 km further away. The lithological

*Corresponding author: zhangy535@mail.sysu.edu.cn

Manuscript received July 13, 2018.
Manuscript accepted November 23, 2018.

structure of the model is represented by a dense grid of approximately 7 million active Lagrangian markers for advecting various material properties and temperatures.

The initial model comprises two continental domains, separated by a low-viscosity weak zone in the top 20 km of the lithospheric mantle to seed the onset of deformation in the numerical models (Fig. 1a). The 120-km-thick continental lithosphere is made up of a 20-km-thick upper crust, a 15-km-thick lower crust and an 85-km-thick lithospheric mantle, overlying the 540-km-thick sublithospheric mantle. We assume that any previously subducted oceanic lithosphere has detached from adjacent continental lithosphere (Van der Voo et al., 1999).

Three different types of continental crustal rheological profile are designed (Figs. 1c–1e), which represent moderate crust, weak crust, and strong crust, respectively. For the moderate crust, the wet quartzite and diabase flow laws are applied for the upper and lower crust, respectively. As comparisons, the wet quartzite and mafic granulite flow laws are applied for the

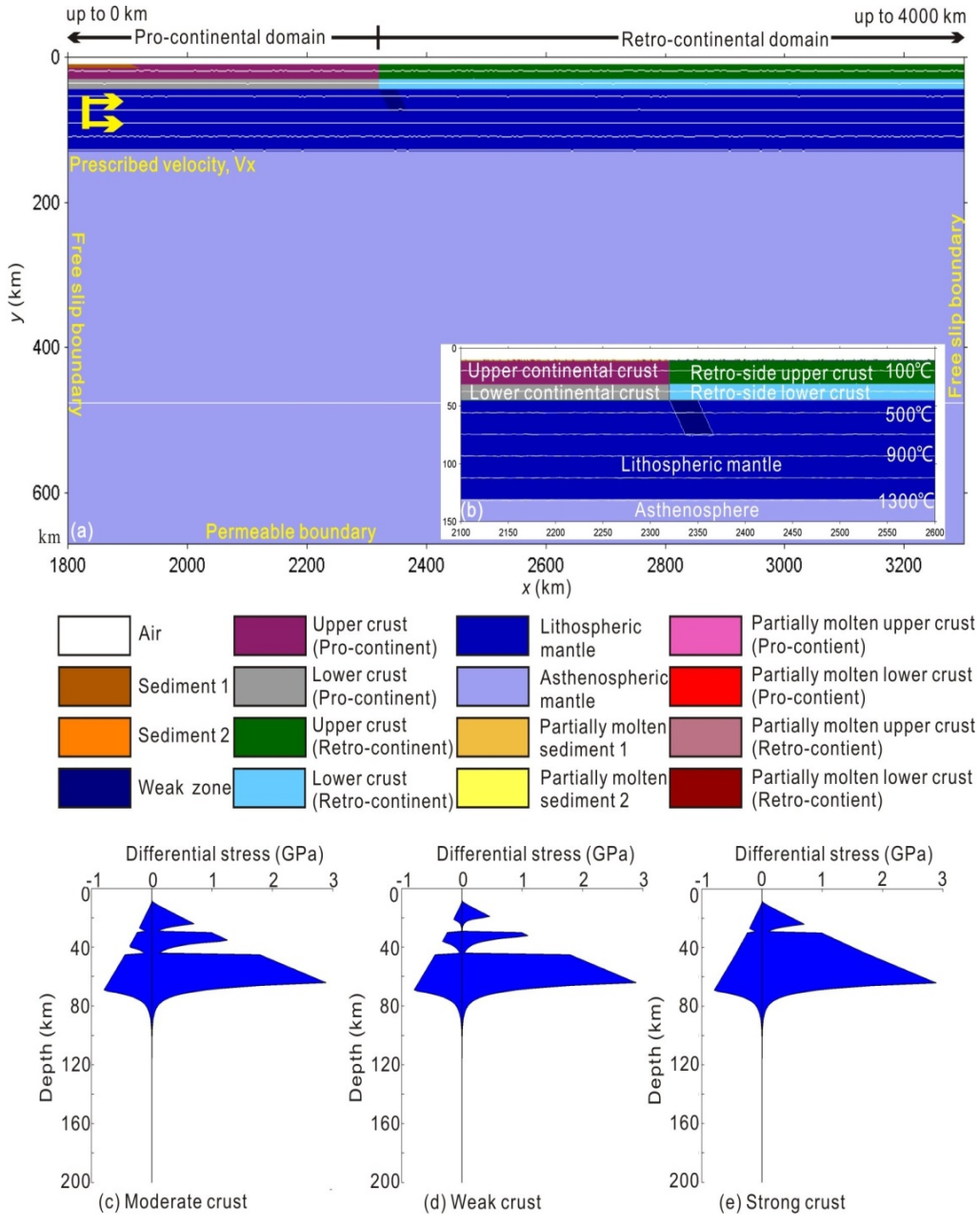

Figure 1. Initial model configuration. (a) Enlargement (1 500×670 km) of the numerical box (4 000×670 km). White lines are isotherms in ºC. Boundary conditions are indicated in yellow. (b) The zoomed domain of the collisional zone. A weak zone is inserted in the upper lithospheric mantle to seed the onset of deformation in the numerical models. Different colors referring to different lithologies and detailed properties are shown in Tables 1 and 2. (c)–(e) Three types of rheological structure of the continental lithosphere are evaluated in this study. They are defined as "moderate crust", "weak crust" and "strong crust", respectively. The upper and lower crust are dominated by wet quartzite and diabase, weakened wet granite and plagioclase, wet quartzite and mafic granulite (Ranalli, 1995), respectively. The lithospheric mantles for all the types conform to the flow law of dry olivine. Rheological strength profiles are computed for a 120-km-thick lithosphere with a Moho temperature of 400 ºC.

upper and lower crust in the strong crust model. In addition, the weak crust model is implemented with wet granite and plagioclase flow laws for the upper and lower crust, respectively; however, the reference viscosities of them are decreased by 0.01 times compared with the corresponding values in Ranalli (1995), in order to highlight the effect of the weak crust on continental collision (Table 1). The flow law of dry olivine is used for the lithospheric mantle and the asthenosphere in all models. The yield-stress envelopes for these different types of continental lithospheres are shown in Figs. 1c–1e. Detailed properties of different rock types are described in Tables 1 and 2.

The boundary conditions used in the models are free slip at all boundaries except the lower boundary, which is treated as permeable to satisfy the free slip of an external boundary at 1 000 km below the base of the model (Ueda et al., 2008; Burg and Gerya, 2005). External free slip conforms to global conservation of mass in the computational domain and is implemented by using the following limitation for velocity components at the lower boundary: $\partial v_x/\partial z = 0$, $\partial v_z/\partial z = -v_z/\Delta z_{\text{external}}$, where $\Delta z_{\text{external}}$ is the vertical distance from the lower boundary to the external boundary where free slip ($\partial v_x/\partial z = 0$, $v_z = 0$) is satisfied. The pushing velocity is assigned to a small internal domain within the pro-side continental lithosphere. Three different convergence rates (1, 3 and 5 cm/yr) are prescribed for different models (Table 3) to explore its effects on the continental collision process. It is worth notifying that the surface is calculated dynamically as an internal free surface by using a buffer layer of "sticky air" (Schmeling et al., 2008). This surface evolves as an erosion/ sedimentation level according to the transport equation (Gerya and Yuen, 2003b).

Table 1 Viscous flow laws used in the numerical experiments

ID	Flow laws	E (kJ·mol^{-1})	V (J·MPa^{-1}·mol^{-1})	n	A_D (MPa^{-n}·s^{-1})	η_0[a] (Pa·s)
A	Air/water	0	0	1.0	1.0×10^{-12}	1.0×10^{12}
B0	Wet quartzite	154	8	2.3	3.2×10^{-4}	1.97×10^{17}
C0	Diabase	260	12	3.4	2.0×10^{-4}	1.26×10^{22}
B1	Wet granite	137	8	1.9	2.0×10^{-2}	1.26×10^{13}
C1	Plagioclase An$_{75}$	238	12	3.2	3.3×10^{-2}	4.8×10^{20}
C2	Mafic granulite	445	12	4.2	1.4×10^{4}	1.13×10^{22}
E	Dry olivine	532	8	3.5	2.5×10^{4}	3.98×10^{16}
F	Wet olivine	470	8	4.0	2.0×10^{3}	5.01×10^{20}
G[b]	Molten felsic	0	0	1.0	2.0×10^{-9}	5.0×10^{14}
H[b]	Molten mafic	0	0	1.0	1.0×10^{-7}	1.0×10^{13}

[a]. η_0 is the reference viscosity, which is calculated: $\eta_0=(1/A_D)\times10^{6n}$; [b]. the molten felsic (G) are used for partial molten sediment and continental upper crust. The molten mafic (H) are used for partial molten continental lower crust. References: Ranalli, 1995; Ji and Zhao, 1993; Kirby and Kronenberg, 1987.

Table 2 Materials properties used in the numerical experiments

Material	State	ρ_0 (kg·m^{-3})	Cp (J·kg^{-1}·K^{-1})	k[a] (W·m^{-1}·K^{-1})	T_{solidus}[b] (K)	T_{liquidus}[b] (K)	Q_L (kJ·kg^{-1})	H_r (μW·m^{-3})	Viscous[c] Flow law	Plastic[d] Sin (φ_{eff})
Sticky air	-	1	100	20	-	-	-	0	A	0
Water	-	1 000	3 330	20	-	-	-	0	A	0
Sediment	Solid	2 700	1 000	K_1	T_{S1}	T_{L1}	300	2.0	B0	0.15
	Molten	2 500	1 500	K_1	T_{S1}	T_{L1}	300	2.0	G	0.06
Continental	Solid	2 700	1 000	K_1	T_{S1}	T_{L1}	300	2.0	B0/B1	0.15
upper crust	Molten	2 500	1 500	K_1	T_{S1}	T_{L1}	300	2.0	G	0.06
Continental	Solid	3 000	1 000	K_2	T_{S2}	T_{L2}	300	0.5	C0/C1/C2	0.15
lower crust	Molten	2 500	1 500	K_2	T_{S2}	T_{L2}	300	0.5	H	0.06
Mantle	Dry	3 300	1 000	K_3	-	-	-	0.022	E	0.6
	Hydrated	3 200	1 000	K_3	-	-	-	0.022	F	0.06
References	-	1, 2	-	3	5	5	1, 2	1	4	-

The thermal expansion coefficient $\alpha=3\times10^{-5}$ K^{-1} and the compressibility coefficient $\beta=1\times10^{-5}$ MPa^{-1} are used for all rock types. [a]. $K_1=[0.64+807/(T_K+77)]\exp(0.000\ 04P_{\text{MPa}})$; $K_2=[1.18+474/(T_K+77)]\exp(0.000\ 04P_{\text{MPa}})$; $K_3=[0.73+1\ 293/(T_K+77)]\exp(0.000\ 04P_{\text{MPa}})$. [b]. $T_{S1}=889+17\ 900/(P+54)+20\ 200/(P+54)^2$, at $P<1\ 200$ MPa; or $831+0.06P$, at $P>1\ 200$ MPa. $T_{L1}=1\ 262+0.09P$; $T_{S2}=973-70\ 400/(P+354)+778\times10^5/(P+354)^2$, at $P<1\ 600$ MPa; or $935+0.003\ 5P+0.000\ 006\ 2P^2$, at $P>1\ 600$ MPa. $T_{L2}=1\ 423+0.105P$. [c]. Parameters of viscous flow laws are shown in Table 1. [d]. The plastic cohesion is zero in all the experiments. φ_{eff} is the effective internal frictional angle implemented for plastic rheology. References: 1. Turcotte and Schubert, 2002; 2. Bittner and Schmeling, 1995; 3. Clauser and Huenges, 1995; 4. Ranalli, 1995; 5. Schmidt and Poli, 1998.

Table 3 Descriptions of the numerical experiments

Models[a]	Pro-side crust type[a]	Retro-side crust type[a]	Convergence rate (cm/yr)	Initial Moho temperatures[b] (ºC)
mm3	Moderate	Moderate	3	400/400
ww3	Weak	Weak	3	400/400
ss3	Strong	Strong	3	400/400
mm1	Moderate	Moderate	1	400/400
mm5	Moderate	Moderate	5	400/400
ww1	Weak	Weak	3	400/400
ww5	Weak	Weak	3	400/400
ss1	Strong	Strong	1	400/400
ss2	Strong	Strong	2	400/400
ss4	Strong	Strong	4	400/400
ss5	Strong	Strong	5	400/400

[a]. Moderate, weak and strong crust are illustrated in Figs. 1c–1e, respectively. [b]. The initial Moho temperatures of pro-side (left value) and retro-side (right value) plates are shown.

Thermal structure of the continental lithosphere is identified with the Moho temperature in this study, which is also dependent on the evaluated models (Table 3). The initial temperature at the surface or at the base of the continental lithospheric mantle is 0 or 1 300 ºC, respectively. The temperature distribution within the continental plate is calculated with linear interpolation from the surface to the Moho (Turcotte and Schubert, 2002). The initial temperature gradient in the asthenospheric mantle is 0.5 ºC/km. The thermal boundary conditions have fixed values for the upper boundary (0 ºC at the surface) and zero horizontal heat flux across the vertical boundaries. For the lower thermal boundary, an infinity-like external constant temperature condition is imposed, which allows both temperature and vertical heat flux to vary along the permeable box lower boundary, ensuring that the constant temperature condition is satisfied at around 1 000 km below the base of the model. This condition is implemented by using the equation $\partial T/\partial z = \left(T_{\text{external}} - T\right)/\Delta z_{\text{external}}$, where T_{external} is the temperature at the external boundary and $\Delta z_{\text{external}}$ is the vertical distance from the lower boundary to the external boundary.

2 MODEL RESULTS

With three different rheological configurations of the continental lithosphere and three different convergence rates, we first constructed 9 numerical experiments. For each of them, the rheological properties of both the pro-plate and retro-plate are the same, and the initial Moho temperature of both plates is set to 400 ºC. The model results demonstrate various modes of continental collision, as shown in the following sections 2.1 and 2.2.

2.1 Models with Variable Crustal Rheological Strength

In this section, 3 numerical models with variable crustal rheological strength have been constructed. The rheological properties of the pro-plate and retro-plate are the same in each model. The convergence rate is 3 cm/yr and keeps constant during the simulation. Detailed parameters of the numerical models can be found in Table 3.

2.1.1 Model with moderate crust

In this model, moderate crust is applied for both the pro-plate and retro-plate. The pro-plate is pushed from the left side by 3 cm/yr, resulting in continuous plate subduction into the asthenosphere. In this process, the bulk of the upper crust is scraped off the slab. The detached crustal materials are accumulated in the collision zone and accreted to the overriding plate. The lower crust can subduct to upper-mantle depths with the continental slab (Fig. 2a). Continuous convergence causes the upper crust of the pro-plate to be progressively detached from the lower crust and thickened, associated with retro-ward migration onto the overriding plate. Thereby, the location of the surface suture between pro-plate and retro-plate diverges from deep subduction zone (Fig. 2b).

After an imposed convergence of larger than 930 km, the subducted lower crust gradually detaches from the slab and exhumes upwards along the subduction channel, under the combined effects of positive buoyancy and mechanical weakening due to thermal conductive heating. In addition, a certain portion of the subducted lower crust intrudes into the mantle wedge and forms a compositionally buoyant and rheologically weak thermal-chemical crustal plume in the sublithospheric depth (Figs. 2c, 2d), the dynamics of which is systematically investigated in Currie et al. (2007) and Li and Gerya (2009). The growth and migration of the sublithospheric crustal plume, in combination with the induced small-scale corner flow, lead to bottom erosion of the overriding lithosphere. At the same time, the detached upper crust of the pro-plate continuously migrates onto the overriding plate, leading to the decoupling of the upper crust of the overriding plate from the lower crust. During this process, the collision zone undergoes significant shear heating and thus large-scale crustal partial melting, where the partially molten rocks tend to extrude upward with forming series of diapiric structures (Fig. 2d). After an imposed convergence of 1 700 km, the surface crustal suture migrates retroward for ~600 km from the initial continental convergent boundary (Fig. 2d). During the convergence, the collision zone uplifts as the detached upper crust is accreted to the overriding plate and thickens in the collision zone, reaching as high as 8

km from the original elevation of 1 km in the subduction zone and forming nearly 4-km-high plateau over the detached crust-migration zone (Fig. 2d). The effective viscosity of the middle crust of the thickened collision zone is particularly low (Fig. 2d) because of the isotherm rising due to crustal thickening and shear heating.

2.1.2 Model with weak crust

In this model, we test the effects of weak crust on the geodynamic processes of continental collision. In this case, the rheological property of the crust is changed from moderate crust to weak crust (Fig. 1d). Under the effects of positive buoyancy and lower crustal rheological strength in this model, a larger amount of the subducted lower crust exhumes upward to the surface along the subduction channel, which is then accumulated in the collision zone and accreted to the overriding plate (Figs. 3a–3b). This can be clearly illustrated through the velocity vector field (Fig. 3b), in which significant crustal exhumation develops along the subduction channel. Although the detached upper crust of the pro-plate can also migrate onto the overriding plate for hundreds of kilometers, crustal partial melting does not occur in the thickened crust, which is quite different from the previous model with moderate crust (c.f., Figs. 2d and 3c). Furthermore, it is worth noting that the bulk of pro-side crust is detached from the slab during collision, with pro-ward migration and thickening, which is clearly expressed in the

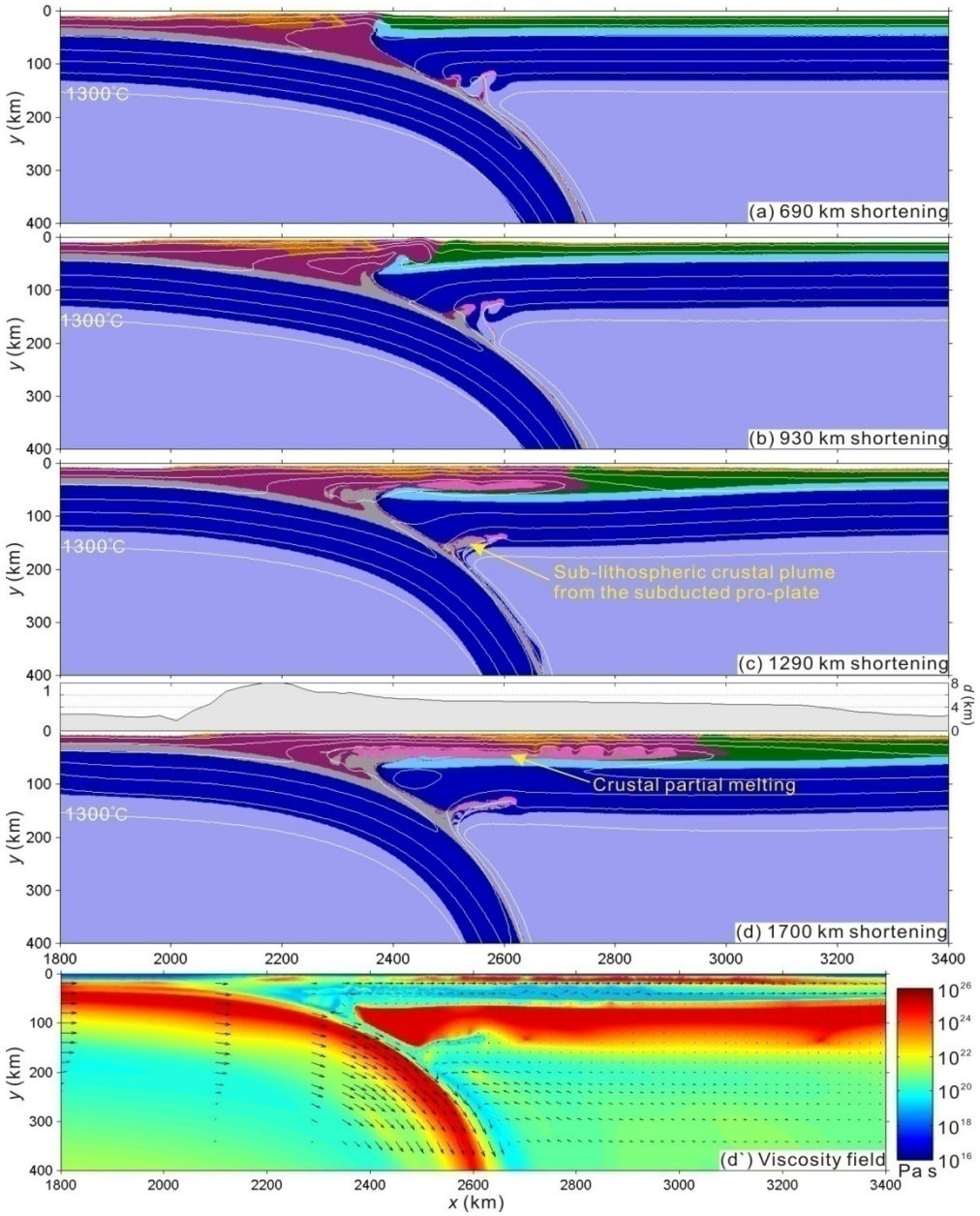

Figure 2. Results of the model with moderate crust (Fig. 1c) and a convergence rate of 3 cm/yr. (a)–(d) Composition and temperature evolution. Colors of rock types are identical to those in Fig. 1a. White numbered lines are isotherms plotted every 200 ºC starting from 100 ºC. The cumulative convergence of the pro-plate is given in each panel. The model surface elevation and the (d`) effective viscosity with velocity vectors are also shown for the final time-step with convergence of 1 700 km.

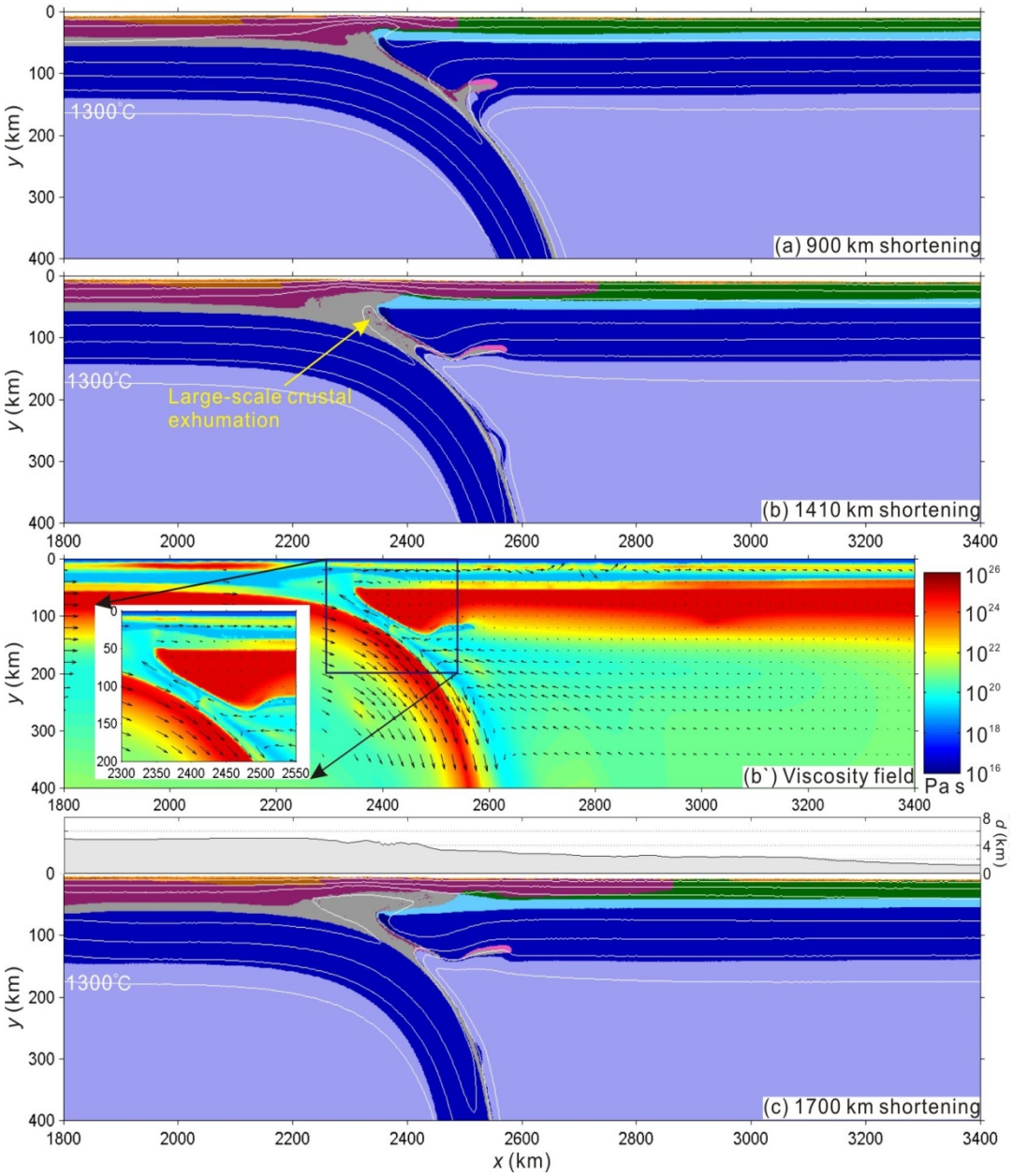

Figure 3. Results of the model with weak crust (Fig. 1d) and a convergence rate of 3 cm/yr. (a)–(c) Composition and temperature evolution. Colors of rock types are identical to those in Fig. 1a. White numbered lines are isotherms plotted every 200 ºC starting from 100 ºC. The cumulative convergence of the pro-plate is given in each panel. The (b`) effective viscosity with velocity vectors is shown for the time-step with cumulative convergence of 1 410 km, highlighting the large-scale crustal exhumation along the subduction channel. The model surface elevation is shown for the final time-step.

resulted high topography of the pro-plate (Fig. 3c).

2.1.3 Model with strong crust

In this model, strong crust (Fig. 1e) is applied for both the pro-plate and retro-plate. The model results, characterized by sub-horizontal underthrusting of the subducting lithosphere beneath the overriding lithosphere, are significantly different from the previous cases with moderate (Fig. 2) or weak crust (Fig. 3). Continuous convergence causes the relatively weak upper crust to be detached from the lower crust and accumulated in the collision zone, which eventually migrates onto the overriding lithosphere (Figs. 4a–4b). Meanwhile, the strong lower crust with a high rheological strength subducts together with the lithospheric mantle. Resulting from the positive buoyancy of subducted lower crust (Fig. 4c), the continental slab gradually bends upward with a decreasing dip angle, eventually leading to the underthrusting of the continental slab directly beneath the overriding lithospheric mantle (Fig. 4c). Similar to the first model with moderate crust, the collision zone is subjected to significant shear heating during the crustal migration, causing partial melting of the thickened upper crust. For the same reason, a broad plateau over the retro-plate has been produced (Fig. 4c). With an imposed convergence of 1 700 km, the length of continental flat-slab can reach ~700 km (Fig. 4c).

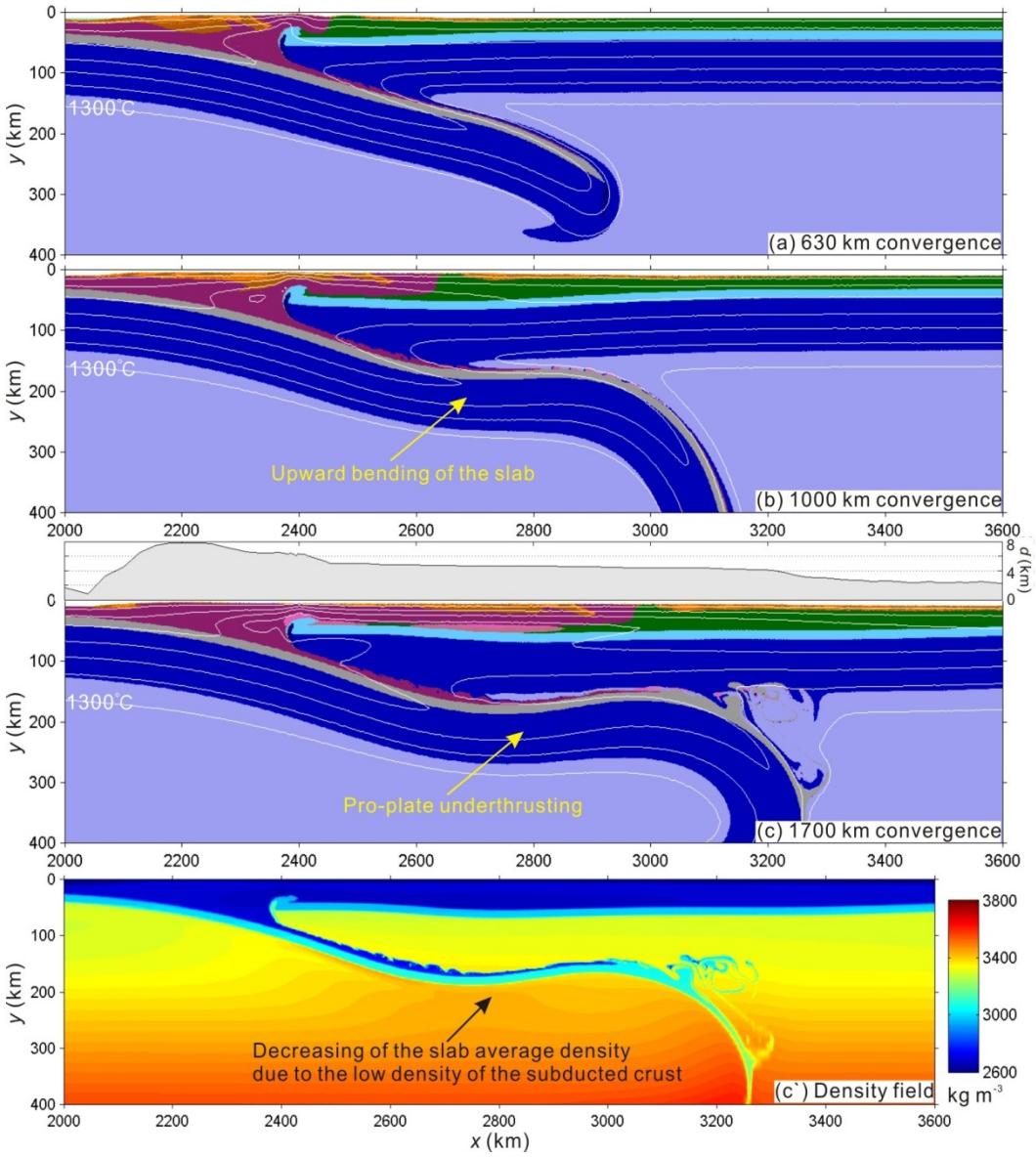

Figure 4. Results of the model with strong crust (Fig. 1e) and a convergence rate of 3 cm/yr. (a)–(c) Composition and temperature evolution. Colors of rock types are identical to those in Fig. 1a. White numbered lines are isotherms plotted every 200 ºC starting from 100 ºC. The cumulative convergence of the pro-plate is given in each panel. The model surface elevation and the (c`) density field are also shown for the final time-step with cumulative convergence of 1 700 km.

2.2 Models with Variable Convergence Rate

In this section, we will decrease the convergence rate to 1 cm/yr or increase to 5 cm/yr for the three previous models with variable crustal rheological strength, in order to further investigate the effects of the convergence rate on the dynamics of continental collision.

2.2.1 Slower or faster collision model with moderate crust

As for the model with moderate crust, we constructed two additional numerical experiments with a lower (1 cm/yr) or a higher (5 cm/yr) convergence rate, in comparison with the previous model with a convergence rate of 3 cm/yr.

When the convergence rate is decreased to 1 cm/yr, the subducting continental plate undergoes sufficient thermal conductive heating and significant mechanical weakening, before it can descend to a larger depth. In combination with the effect of crustal buoyancy, it greatly contributes to large-scale exhumation of the subducted lower crust along the subduction channel (Fig. 5a), which further facilitates the migration of the detached crust of the pro-plate onto the overriding lithosphere, as well as the asthenospheric upwelling in the collision zone (Fig. 5b). It is worth noting that the downgoing slab experiences repeated break-off at the depth of ~400 km (Figs. 5b–5d), which is mainly due to the higher Stokes sinking velocity, induced by negative buoyancy of the slab, than the prescribed low plate convergence velocity. In addition, the subducting lithosphere retreats slowly with the delamination of crustal materials from the underlying lithospheric mantle, which is accompanied by the asthenospheric upwelling. The effective viscosity and the velocity field in the subduction zone clearly shows the mechanical weakening and successive detachment of the slab as well as the progressive retreat of the pro-plate (Fig. 6). The

asthenospheric upwelling along the subduction channel is highlighted in Fig. 6b. In this model, the sub-lithospheric crustal plume originating from the subducted crust is not formed, because very limited crustal material can subduct to asthenospheric depths, compared to the counterpart model with a convergence rate of 3 cm/yr.

When the convergence rate is increased to 5 cm/yr, the model result is generally similar to the model with a convergence rate of 3 cm/yr, although the high convergence rate may lead to a larger amount of upper crust subducted into the channel.

2.2.2 Slower or faster collision model with weak crust

In order to test the effects of the convergence rate on the model with weak crust, we similarly constructed two numerical experiments with a lower (1 cm/yr) or a higher (5 cm/yr) convergence rate, in comparison with the previous model with a convergence rate of 3 cm/yr.

At a lower convergence rate (1 cm/yr), the mechanical deformation of the collision zone is mainly controlled by conductive heat transfer. In this case, the slab undergoes significant mechanical weakening. As a result, this model is characterized by successive break-off of the subducting slab at the depth of ~200 km due to the relatively higher Stokes sinking velocity than the prescribed subduction velocity, which is the largest difference from the previous model with a convergence rate of 3 cm/yr (cf., Figs. 3 and 7). Continuous convergence causes almost the whole crust to be detached from the subducting slab and accumulated in the collision zone. The thickening of the pro-side crust in the collision zone absorbs most of the crustal deformation, due to the low crustal rheological strength and the low convergence rate, which thereby does not deform the overriding lithosphere significantly (Fig. 7).

When the convergence rate is increased to 5 cm/yr, the model result is generally similar to the model with a conver-

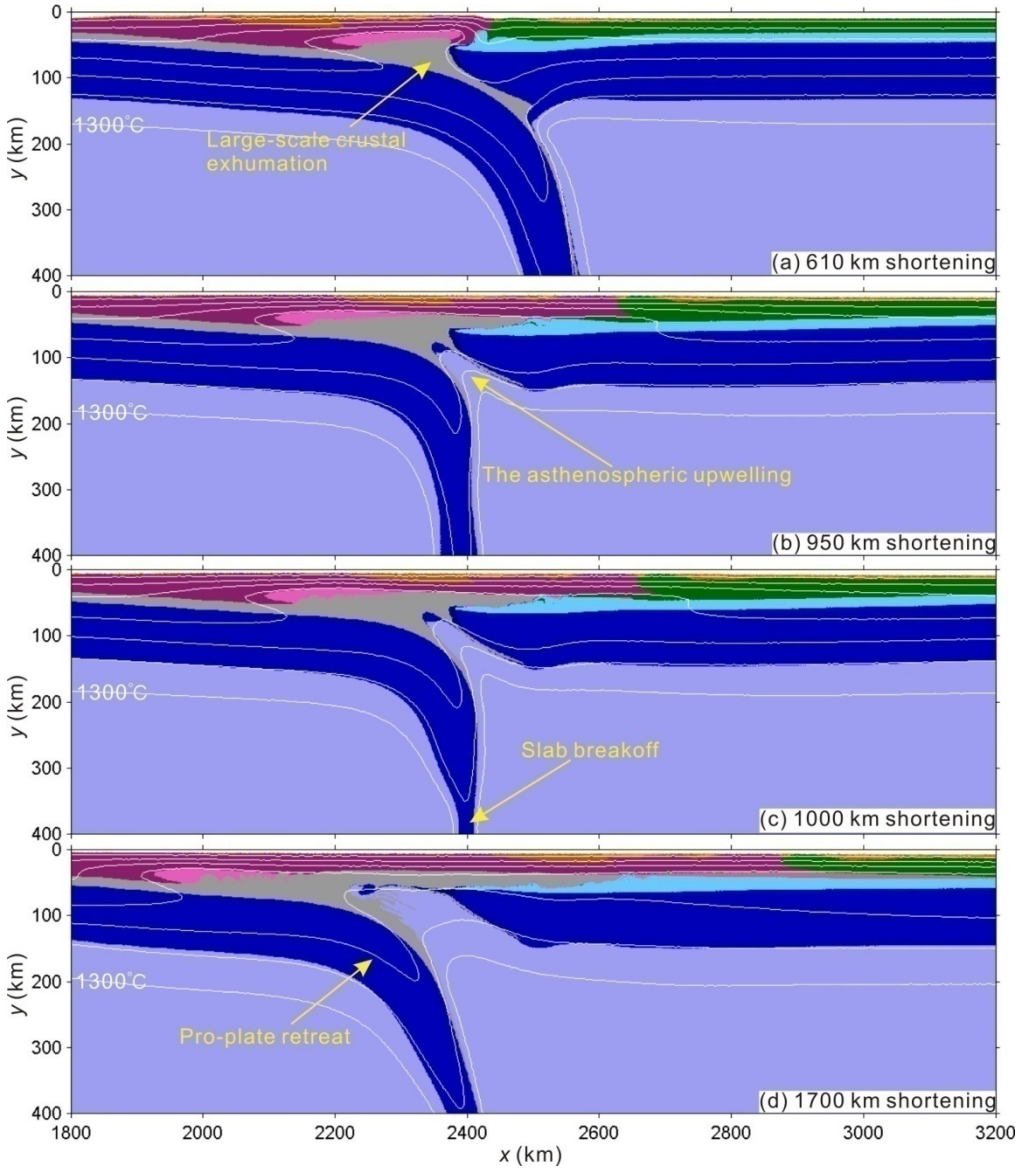

Figure 5. Results of the model with moderate crust (Fig. 1c) and a low convergence rate of 1 cm/yr. (a)–(d) Composition and temperature evolution. Colors of rock types are identical to those in Fig. 1a. White numbered lines are isotherms plotted every 200 ºC starting from 100 ºC. The cumulative convergence of the pro-plate is given in each panel.

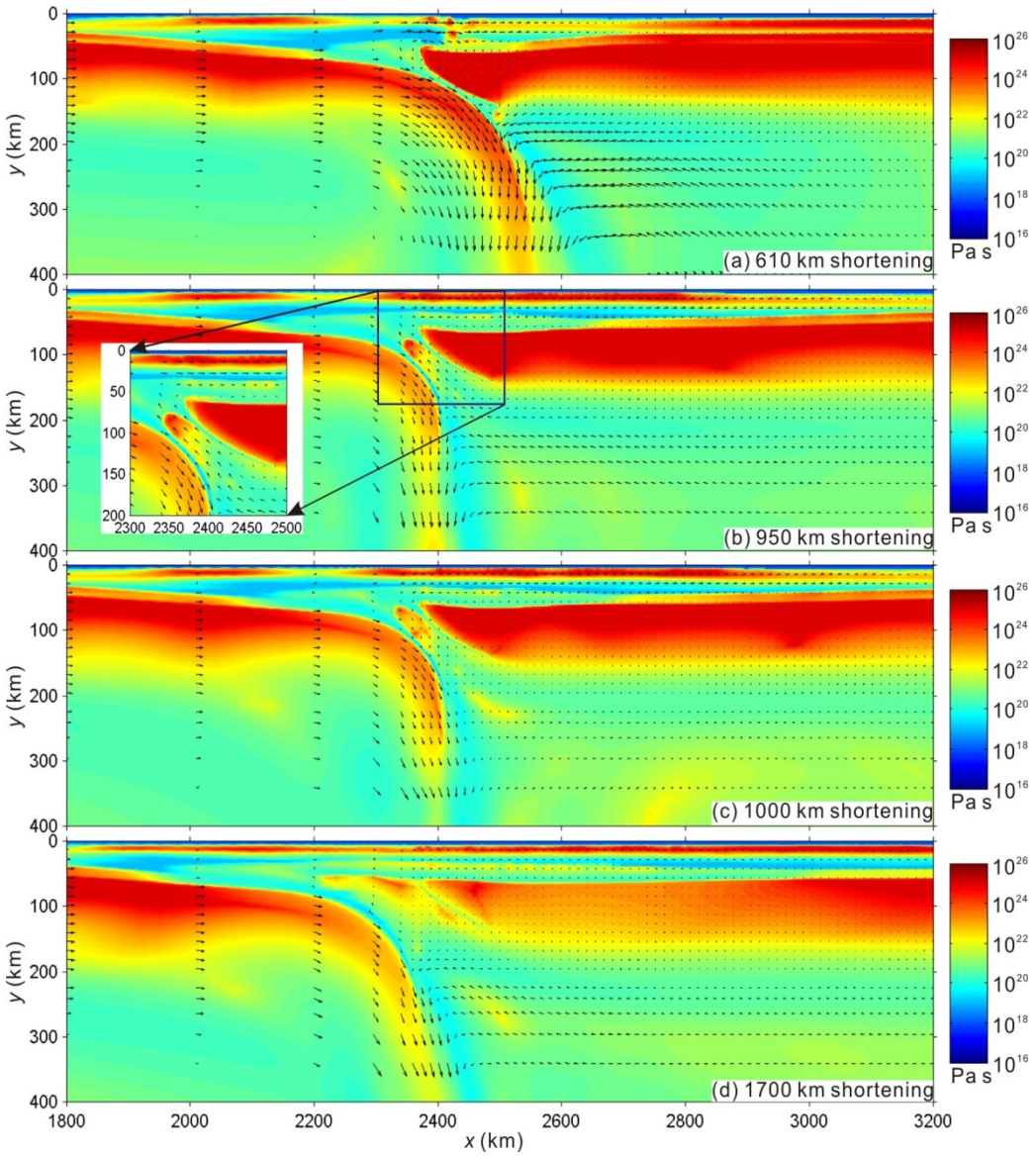

Figure 6. Evolution of the effective viscosity and velocity vectors for the same model as in Fig. 5. The cumulative convergence of the pro-plate is given in each panel. In (b), the large-scale crustal exhumation and the asthenospheric upwelling along the initial subduction channel are highlighted in the inset figure.

gence rate of 3 cm/yr, although the higher convergence rate inhibits large-scale crustal exhumation and plate decoupling along the subduction channel.

2.2.3 Slower or faster collision model with strong crust

As shown in Fig. 4, continental flat-slab subduction develops in the model with strong crust and a convergence rate of 3 cm/yr. In order to explore its correlation with variable convergence rate, four additional models are constructed, in which the convergence rate is decreased to 1 or 2 cm/yr or increased to 4 or 5 cm/yr. Results of all the five models (including the previous model with a convergence rate of 3 cm/yr) with strong crust and variable convergence rate are illustrated in Fig. 8, which shows the model snapshots with the same convergence of 1 700 km.

The model results indicate that the convergence rate can greatly affect the mode of continental subduction. As for the models with a convergence rate of ≤2 cm/yr, the continental slab continuously subducts into the deep mantle at a steep angle (Figs. 8a–8b). The model with the lowest convergence rate of 1 cm/yr is characterized by a ~200 km retreat of the pro-plate with the asthenospheric upwelling along the subduction channel (Fig. 8a). In addition, remarkable destruction of the bottom of the overriding lithospheric mantle takes place in the models with a convergence rate of ≤2 cm/yr, which is caused by the growth and migration of partially molten plumes originating from the subducted crust as well as the induced mantle flow. When the convergence velocity is increased to ≥3 cm/yr, continental flat-slab subduction is resulted (Figs. 8c–8e). The length of flat-slab is positively correlated to the convergence rate, as shown in Figs. 8c–8e.

Based on the corresponding stress fields of the five models at an equal convergence of 1 700 km (Figs. 9a–9e), it indicates that the continental subduction mode might be dependent on the stress that the subducting slab can support. When the convergence rate is low (≤2 cm/yr), the continental slab stays in

the hot asthenosphere for a relatively longer time, which results in significant thermal conductive heating and mechanical weakening. In these cases, the slab cannot support large stress for the continuous flat subduction, which thereby results in slab rollback and steep subduction (Figs. 9a–9b). In contrast, when the convergence rate is increased to larger than 3 cm/yr, the subducted slab can maintain its rheological strength and thus can support the large stress facilitating a low-angle subduction (Figs. 9c–9e). In addition, the whole lower crust together with a certain amount of upper crust of the pro-plate can subduct into the asthenosphere in the models with higher convergence rate, which will decrease the average density of the slab. Both conditions contribute to the formation of continental flat-slab subduction.

3 DISCUSSION

Our numerical simulations reveal three basic modes of continental subduction, including slab break-off, steep subduction and continental flat-slab subduction. Both the first two modes can be further divided into two sub-types, according to the development of pro-side lithospheric mantle retreat or not. On the basis of the numerical results, we further constructed a regime diagram to illustrate how the continental subduction mode correlates with the crustal rheological strength of the converging plates and the convergence rate (Fig. 10).

For the first mode of slab break-off, the subducting continental plate is successively detached from the pro-plate and sinks into the deep mantle under the conditions of low/moderate rheological strength of the continental crust and low convergence rate (Fig. 10). Weak/moderate crust directly decreases the average rheological strength of the pro-plate lithosphere. In addition, the low convergence rate causes the subducting slab staying in the hot asthenospheric mantle for longer time and thus undergoing sufficient thermal conductive heating. Both conditions contribute to significant mechanical weakening of the subducting slab, thereby facilitating progressive slab break-off. In these cases, the development of pro-plate retreat or not is mainly controlled by the thickness and rheological

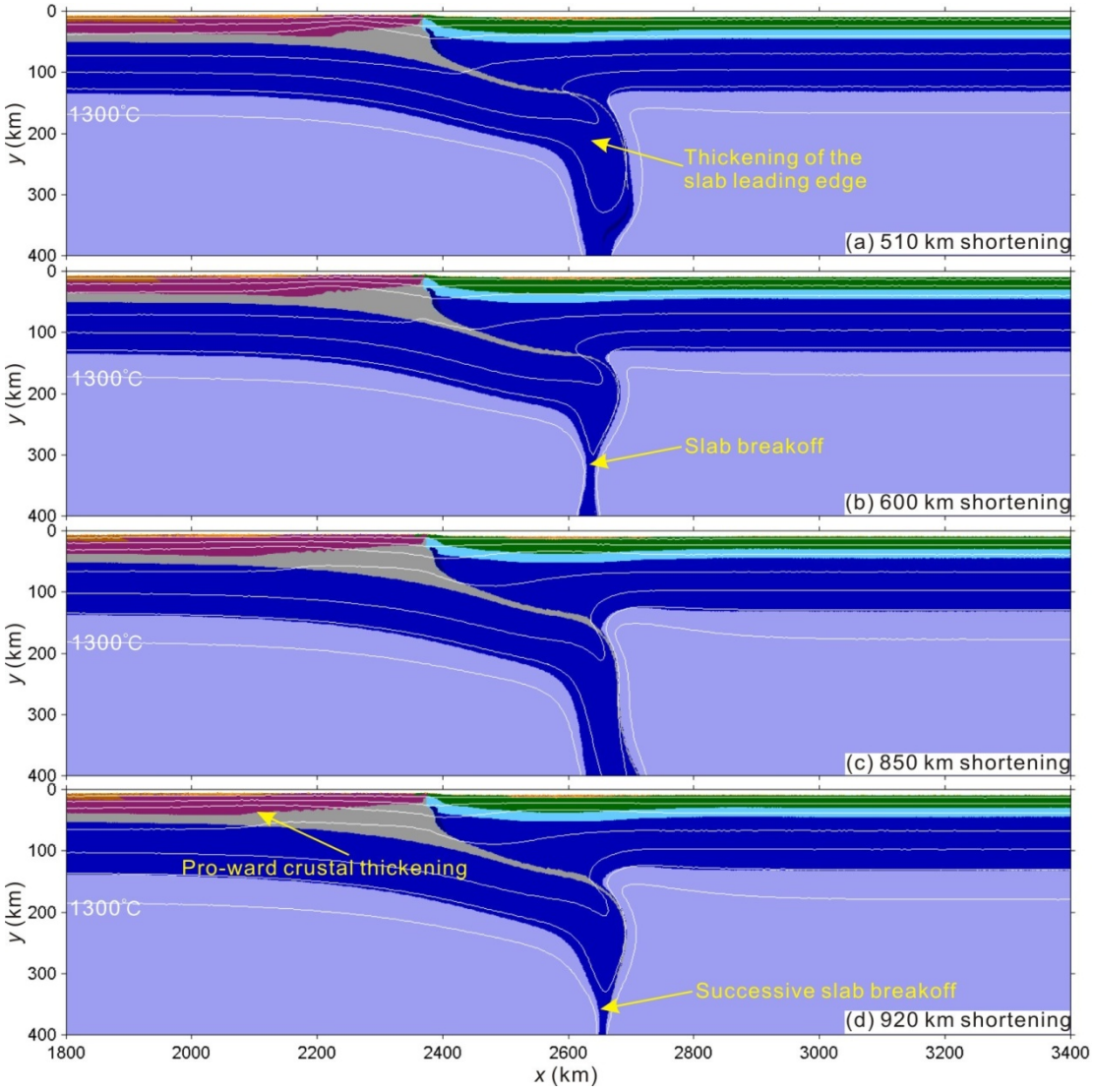

Figure 7. Results of the model with weak crust (Fig. 1d) and a low convergence rate of 1 cm/yr. (a)–(d) Composition and temperature evolution. Colors of rock types are identical to those in Fig. 1a. White numbered lines are isotherms plotted every 200 ºC starting from 100 ºC. The cumulative convergence of the pro-plate is given in each panel.

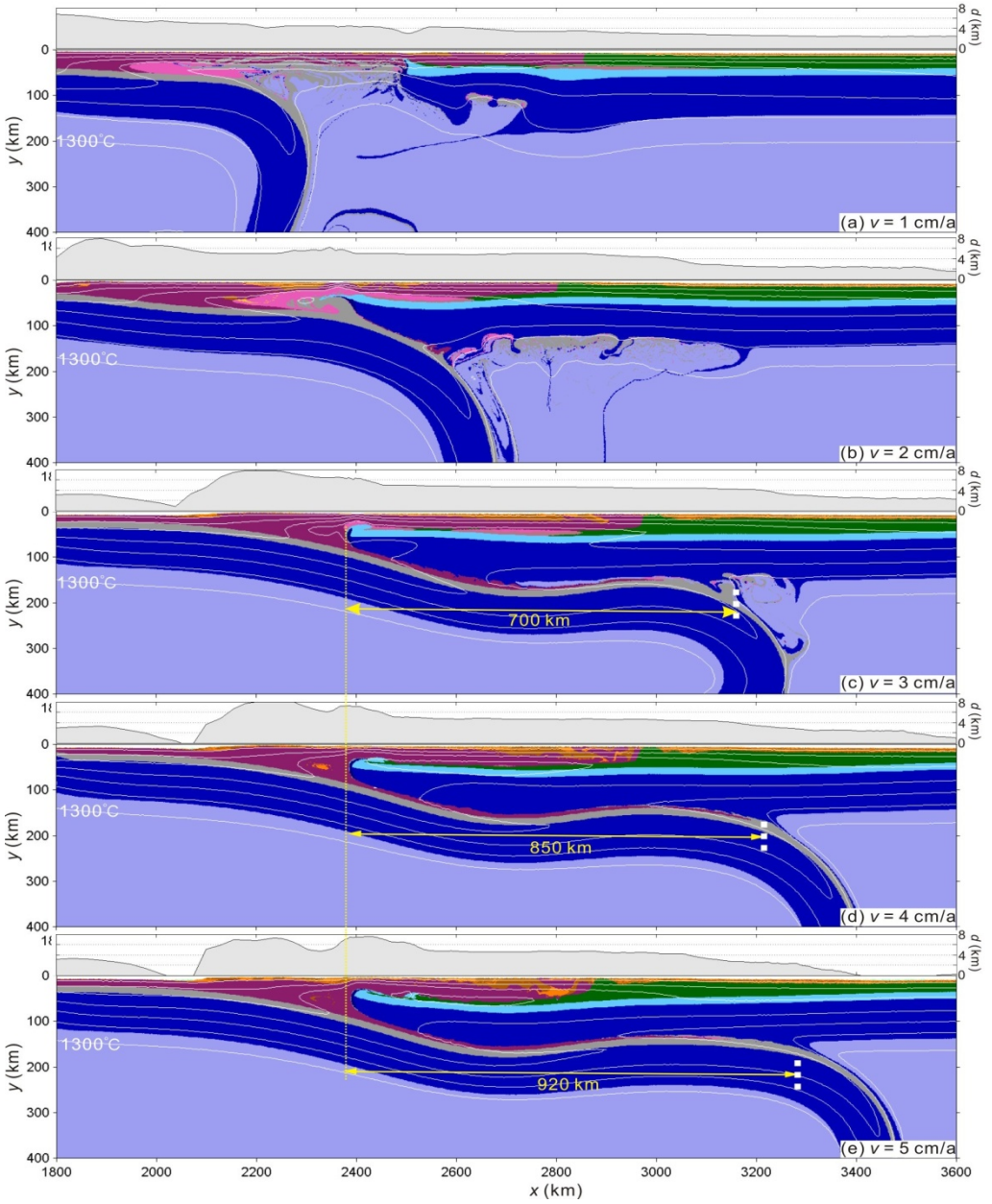

Figure 8. Effects of the convergence rate in the models with strong crust (Fig. 1e). From (a) to (e), when the convergence rate is linearly increased from 1 to 5 cm/yr. All the simulations stopped at a cumulative convergence of 1 700 km. Colors of rock types are identical to those in Fig. 1a. White numbered lines are isotherms plotted every 200 ºC starting from 100 ºC. The corresponding model surface elevation is also shown above in each panel.

strength of the subduction channel, which strongly affect the plate (de)coupling. If the crustal rheological strength is low, almost the whole crust of the pro-plate is scraped off the slab and accumulated in the collision zone (Fig. 7). Thereby, very few lower crustal rocks enter the deeper subduction channel, which leads to strong coupling between the subducting and overriding plates, and thus prevents the pro-plate retreat. However, when the crustal rheological strength is increased to moderate, more crustal rocks can be dragged into the deeper subduction channel (Fig. 5). Consequently, a thicker and weaker subduction channel is formed, which decouples the converging plates and may further contribute to the pro-plate retreat, asthenospheric upwelling and subsequent large-scale crustal exhumation. The geodynamic processes of this mode may be comparable to the continental collision in the Southeast Carpathians, Romania, where relevant studies indicated the development of gravitational instabilities in the Carpathians collision zone (Cloetingh et al., 2004). The presence of two high-velocity bodies in the upper mantle inferred from seismic tomography studies (Wortel and Spakman, 2000; Radulescu, 1988) might be resulted from progressive slab detachment as illustrated in Fig. 7.

In contrast to the slab break-off mode, continental flat-slab subduction favors the opposite conditions, e.g., strong crust and high convergence rate (Fig. 10). Both strong crust and high convergence rate can increase the average rheological strength of the continental slab, which contributes to the development of a low-angle subduction. Meanwhile, in this case, larger amount

of continental crust can be subducted into the asthenosphere, which will greatly decrease the average density of the slab and thus induce its upward bending. Eventually, the subducting slab would underplate the overriding lithosphere, as shown in Fig. 4. This mode might be well represented by the Himalayan-Tibetan orogen (Zhang et al., 2018; Chen et al., 2015; Zhao et al., 2010; Nábělek et al., 2009; Li et al., 2008; Tilmann and Ni, 2003; Owens and Zandt, 1997).

The mode of steep subduction is developed in the other conditions (Fig. 10). Specifically, under the condition of low crustal rheological strength with high convergence rate, a typical steep subduction is developed, together with retro-ward migration of the detached crust onto the overriding lithosphere, the formation of sublithospheric crustal plumes and the bottom erosion of the overriding lithosphere (e.g., Fig. 2). However, the condition of high crustal rheological strength with low convergence rate can also result in steep subduction, which is accompanied with significant pro-plate retreat resulting from the higher Stokes sinking velocity than the prescribed low convergence rate. The typical steep subduction might develop in many current collision zones in nature, such as the Dabie-Sulu orogen in eastern China (Li Z Y et al., 2018; Dai et al., 2016; Zheng et al., 2008). As for the steep subduction with pro-plate retreat, a possible analog is the northern Apennines, where the subducted Adria micro-continental lithosphere experienced eastward retreat accompanying an obvious delamination of the subducted lithosphere with its overlying continental crust (Chiarabba et al., 2014; Chiarabba and Chiodini, 2013; Faccenda et al., 2008).

4 CONCLUSIONS

We have constructed high-resolution thermo-mechanical

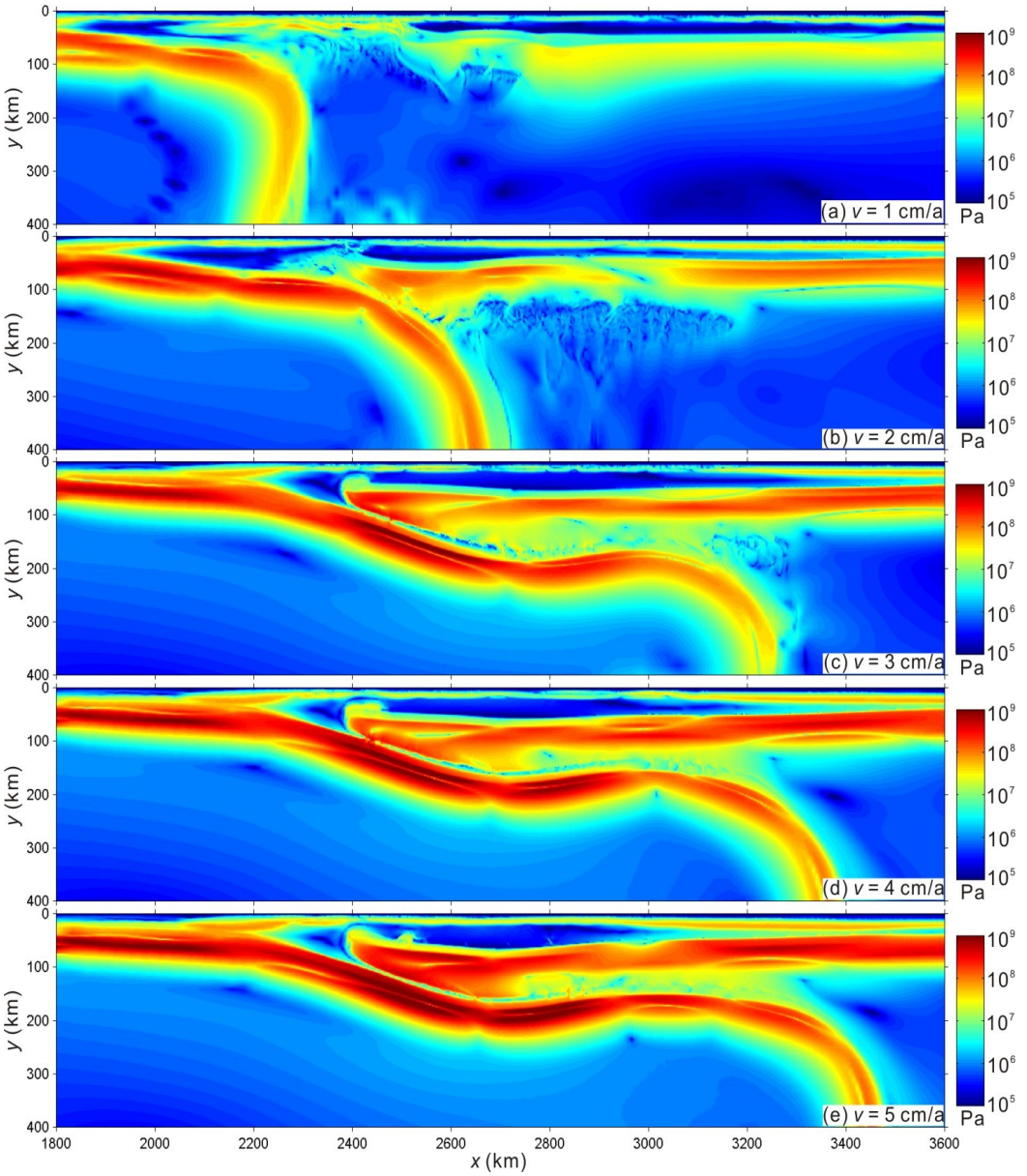

Figure 9. The stress fields (the second invariant of deviatoric stress) are shown for the same model as in Fig. 8. All the simulations stopped at a cumulative convergence of 1 700 km.

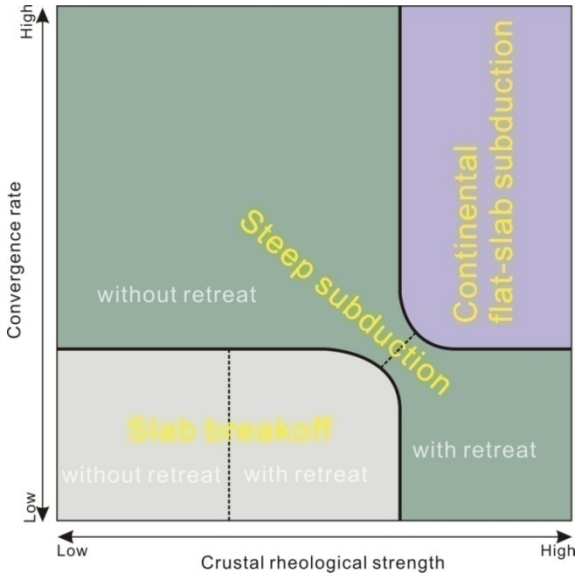

Figure 10. Dependence of continental subduction mode on the crustal rheological strength and the convergence rate. It indicates that continental subduction can be classified into three basic modes including slab breakoff, steep subduction and continental flat-slab subduction. The first two modes can be further divided into two sub-types, according to the development of pro-side lithospheric mantle retreat or non-retreat. The regime diagram is established based on the models with the same crustal rheological profile for both the pro-plate and retro-plate, in which the initial Moho temperatures are 400 ºC.

numerical models to systematically investigate the dynamics of continental subduction during continental convergence. If the pro-plate and retro-plate share the same thermal structure with an initial Moho temperature of 400 ºC, continental subduction can be classified into three basic modes including slab breakoff, steep subduction and continental flat-slab subduction, depending on the crustal rheology and the convergence rate.

Weak crust and low convergence rate favor slab detachment. Strong crust and high convergence rate result in continental flat-slab subduction. Otherwise, steep subduction is developed. In addition, the low convergence rate may greatly contribute to the retreat of subducting plate.

ACKNOWLEDGMENTS

This work was supported by the Strategic Priority Research Program (B) of Chinese Academy of Sciences (No. XDB18000000), the NSFC Project (Nos. 41622404, 41688103, U1701641 and 41704091), the 973 Project (No. 2015CB856106). Numerical simulations were run with the clusters of National Supercomputer Center in Guangzhou (Tianhe-II). The final publication is available at Springer via https://doi.org/10.1007/s12583-017-0946-y.

REFERENCES CITED

Bittner, D., Schmeling, H., 1995. Numerical Modelling of Melting Processes and Induced Diapirism in the Lower Crust. *Geophysical Journal International*, 123(1): 59–70. https://doi.org/10.1111/j.1365-246x.1995.tb06661.x

Burg, J. P., Podladchikov, Y., 2000. From Buckling to Asymmetric Folding of the Continental Lithosphere: Numerical Modelling and Application to the Himalayan Syntaxes. *Geological Society*, *London*, *Special Publications*, 170(1): 219–236. https://doi.org/10.1144/gsl.sp.2000.170.01.12

Burg, J. P., Gerya, T. V., 2005. The Role of Viscous Heating in Barrovian Metamorphism of Collisional Orogens: Thermomechanical Models and Application to the Lepontine Dome in the Central Alps. *Journal of Metamorphic Geology*, 23(2): 75–95. https://doi.org/10.1111/j.1525-1314.2005.00563.x

Burov, E., Francois, T., Yamato, P., et al., 2014a. Mechanisms of Continental Subduction and Exhumation of HP and UHP Rocks. *Gondwana Research*, 25(2): 464–493. https://doi.org/10.1016/j.gr.2012.09.010

Burov, E., Francois, T., Agard, P., et al., 2014b. Rheological and Geodynamic Controls on the Mechanisms of Subduction and HP/UHP Exhumation of Crustal Rocks during Continental Collision: Insights from Numerical Models. *Tectonophysics*, 631: 212–250. https://doi.org/10.1016/j.tecto.2014.04.033

Burov, E. B., Molnar, P., 1998. Gravity Anomalies over the Ferghana Valley (Central Asia) and Intracontinental Deformation. *Journal of Geophysical Research*: *Solid Earth*, 103(B8): 18137–18152. https://doi.org/10.1029/98jb01079

Chen, Y., Li, W., Yuan, X. H., et al., 2015. Tearing of the Indian Lithospheric Slab beneath Southern Tibet Revealed by SKS-Wave Splitting Measurements. *Earth and Planetary Science Letters*, 413: 13–24. https://doi.org/10.1016/j.epsl.2014.12.041

Chiarabba, C., Chiodini, G., 2013. Continental Delamination and Mantle Dynamics Drive Topography, Extension and Fluid Discharge in the Apennines. *Geology*, 41(6): 715–718. https://doi.org/10.1130/g33992.1

Chiarabba, C., Giacomuzzi, G., Bianchi, I., et al., 2014. From Underplating to Delamination-Retreat in the Northern Apennines. *Earth and Planetary Science Letters*, 403: 108–116. https://doi.org/10.1016/j.epsl.2014.06.041

Clauser, C., Huenges, E., 1995. Thermal Conductivity of Rocks and Minerals. *AGU Reference Shelf*, 3: 105–126. http://doi.10.1029/RF003p0105

Cloetingh, S., Burov, E., Poliakov, A., 1999. Lithosphere Folding: Primary Response to Compression? (From Central Asia to Paris Basin). *Tectonics*, 18(6): 1064–1083. https://doi.org/10.1029/1999tc900040

Cloetingh, S. A. P. L., Burov, E., Matenco, L., et al., 2004. Thermo-Mechanical Controls on the Mode of Continental Collision in the SE Carpathians (Romania). *Earth and Planetary Science Letters*, 218(1/2): 57–76. https://doi.org/10.1016/s0012-821x(03)00645-9

Conrad, C. P., Molnar, P., 1997. The Growth of Rayleigh-Taylor-Type Instabilities in the Lithosphere for Various Rheological and Density Structures. *Geophysical Journal International*, 129(1): 95–112. https://doi.org/10.1111/j.1365-246x.1997.tb00939.x

Currie, C. A., Beaumont, C., Huismans, R. S., 2007. The Fate of Subducted Sediments: A Case for Backarc Intrusion and Underplating. *Geology*, 35(12): 1111. https://doi.org/10.1130/g24098a.1

Dai, L. Q., Zheng, Y. F., He, H. Y., et al., 2016. Postcollisional Mafic Igneous Rocks Record Recycling of Noble Gases by Deep Subduction of the Continental Crust. *Lithos*, 252/253: 135–144. https://doi.org/10.1016/j.lithos.2016.02.025

Faccenda, M., Gerya, T. V., Chakraborty, S., 2008. Styles of Post-Subduction Collisional Orogeny: Influence of Convergence Velocity, Crustal Rheology and Radiogenic Heat Production. *Lithos*, 103(1/2): 257–287. https://doi.org/10.1016/j.lithos.2007.09.009

Gerya, T. V., Yuen, D. A., 2003a. Rayleigh-Taylor Instabilities from Hydration and Melting Propel 'Cold Plumes' at Subduction Zones. *Earth and Planetary Science Letters*, 212(1/2): 47–62. https://doi.org/10.1016/s0012-821x(03)00265-6

Gerya, T. V., Yuen, D. A., 2003b. Characteristics-Based Marker-in-Cell Method with Conservative Finite-Differences Schemes for Modeling

Geological Flows with Strongly Variable Transport Properties. *Physics of the Earth and Planetary Interiors*, 140(4): 293–318. https://doi.org/10.1016/j.pepi.2003.09.006

Gray, R., Pysklywec, R. N., 2012. Geodynamic Models of Mature Continental Collision: Evolution of an Orogen from Lithospheric Subduction to Continental Retreat/Delamination. *Journal of Geophysical Research*: *Solid Earth*, 117(B3). https://doi.org/10.1029/2011jb008692

Houseman, G. A., Molnar, P., 1997. Gravitational (Rayleigh-Taylor) Instability of a Layer with Non-Linear Viscosity and Convective Thinning of Continental Lithosphere. *Geophysical Journal International*, 128(1): 125–150. https://doi.org/10.1111/j.1365-246x.1997.tb04075.x

Huangfu, P. P., Wang, Y. J., Fan, W. M., et al., 2017. Dynamics of Unstable Continental Subduction: Insights from Numerical Modeling. *Science China*: *Earth Sciences*, 60(2): 218–234. https://doi.org/10.1007/s11430-016-5014-6

Ji, S. C., Zhao, P. L., 1993. Flow Laws of Multiphase Rocks Calculated from Experimental Data on the Constituent Phases. *Earth and Planetary Science Letters*, 117(1/2): 181–187. https://doi.org/10.1016/0012-821x(93)90125-s

Kirby, S. H., Kronenberg, A. K., 1987. Rheology of the Lithosphere: Selected Topics. *Reviews of Geophysics*, 25(6): 1219–1244. https://doi.org/10.1029/rg025i006p01219

Li, C., Van der Hilst, R. D., Meltzer, A. S., et al., 2008. Subduction of the Indian Lithosphere beneath the Tibetan Plateau and Burma. *Earth and Planetary Science Letters*, 274(1/2): 157–168. https://doi.org/10.1016/j.epsl.2008.07.016

Li, F. C., Sun, Z., Zhang, J. Y., 2018. Numerical Studies on Continental Lithospheric Breakup in Response to the Extension Induced by Subduction Direction Inversion. *Earth Scinece*, 43(10): 3762–3777 (in Chinese with English Abstract)

Li, Z. H., Gerya, T. V., 2009. Polyphase Formation and Exhumation of High- to Ultrahigh-Pressure Rocks in Continental Subduction Zone: Numerical Modeling and Application to the Sulu Ultrahigh-Pressure Terrane in Eastern China. *Journal of Geophysical Research*, 114(B9): B09406. https://doi.org/10.1029/2008jb005935

Li, Z. H., Gerya, T. V., Burg, J. P., 2010. Influence of Tectonic Overpressure OnP-Tpaths of HP-UHP Rocks in Continental Collision Zones: Thermomechanical Modelling. *Journal of Metamorphic Geology*, 28(3): 227–247. https://doi.org/10.1111/j.1525-1314.2009.00864.x

Li, Z. H., Xu, Z. Q., Gerya, T. V., 2011. Flat versus Steep Subduction: Contrasting Modes for the Formation and Exhumation of High- to Ultrahigh-Pressure Rocks in Continental Collision Zones. *Earth and Planetary Science Letters*, 301(1/2): 65–77. https://doi.org/10.1016/j.epsl.2010.10.014

Li, Z. H., 2014. A Review on the Numerical Geodynamic Modeling of Continental Subduction, Collision and Exhumation. *Science China*: *Earth Sciences*, 57(1): 47–69. https://doi.org/10.1007/s11430-013-4696-0

Li, Z. Y., Li, Y. L., Wijbrans, J. R., et al., 2018. Metamorphic *P-T* Path Differences between the Two UHP Terranes of Sulu Orogen, Eastern China: Petrologic Comparison between Eclogites from Donghai and Rongcheng. *Journal of Earth Science*, 29(5): 1151–1166. https://doi.org/10.1007/s12583-018-0845-x

Nabelek, J., Hetenyi, G., Vergne, J., et al., 2009. Underplating in the Himalaya-Tibet Collision Zone Revealed by the HI-CLIMB Experiment. *Science*, 325(5946): 1371–1374. https://doi.org/10.1126/science.1167719

Owens, T. J., Zandt, G., 1997. Implications of Crustal Property Variations for Models of Tibetan Plateau Evolution. *Nature*, 387(6628): 37–43. https://doi.org/10.1038/387037a0

Radulescu, F., 1988. Seismic Models of the Crustal Structure in Romania. *Rev. Roum. Geol. Geophys. Geogr. Ser. Geophys*, 32: 13–17

Ranalli, G., 1995. Rheology of the Earth. Springer, Berlin. https://doi.org/10.1016/s0040-1951(96)00042-x

Schmeling, H., Babeyko, A. Y., Enns, A., et al., 2008. A Benchmark Comparison of Spontaneous Subduction Models—Towards a Free Surface. *Physics of the Earth and Planetary Interiors*, 171(1/2/3/4): 198–223. https://doi.org/10.1016/j.pepi.2008.06.028

Schmidt, M. W., Poli, S., 1998. Experimentally Based Water Budgets for Dehydrating Slabs and Consequences for Arc Magma Generation. *Earth and Planetary Science Letters*, 163(1/2/3/4): 361–379. https://doi.org/10.1016/s0012-821x(98)00142-3

Tilmann, F., Ni, j., 2003. Seismic Imaging of the Downwelling Indian Lithosphere beneath Central Tibet. *Science*, 300(5624): 1424–1427. https://doi.org/10.1126/science.1082777

Turcotte, D. L., Schubert, G., 2002. Geodynamics. Cambridge University Press, Cambridge. http://doi.10.1017/cbo9780511807442

Ueda, K., Gerya, T., Sobolev, S. V., 2008. Subduction Initiation by Thermal-Chemical Plumes: Numerical Studies. *Physics of the Earth and Planetary Interiors*, 171(1/2/3/4): 296–312. https://doi.org/10.1016/j.pepi.2008.06.032

Van der Voo, R., Spakman, W., Bijwaard, H., 1999. Tethyan Subducted Slabs under India. *Earth and Planetary Science Letters*, 171(1): 7–20. https://doi.org/10.1016/s0012-821x(99)00131-4

Warren, C. J., 2013. Exhumation of (Ultra-)High-Pressure Terranes: Concepts and Mechanisms. *Solid Earth*, 4(1): 75–92. https://doi.org/10.5194/se-4-75-2013

Wortel, M. J. R., Spakman, W., 2000. Subduction and Slab Detachment in the Mediterranean-Carpathian Region. *Science*, 290(5498): 1910–1917. https://doi.org/10.1126/science.290.5498.1910

Zhang, L., Ye, Y., Qin, S., et al., 2018. Water in the Thickened Lower Crust of the Eastern Himalayan Orogen. *Journal of Earth Science*, 29(5): 1040–1048. https://doi.org/10.1007/s12583-018-0880-7

Zhao, J. M., Yuan, X. H., Liu, H. B., et al., 2010. The Boundary between the Indian and Asian Tectonic Plates below Tibet. *Proceedings of the National Academy of Sciences*, 107(25): 11229–11233. https://doi.org/10.1073/pnas.1001921107

Zheng, J. P., Sun, M., Griffin, W. L., et al., 2008. Age and Geochemistry of Contrasting Peridotite Types in the Dabie UHP Belt, Eastern China: Petrogenetic and Geodynamic Implications. *Chemical Geology*, 247(1/2): 282–304. https://doi.org/10.1016/j.chemgeo.2007.10.023